AD-A112 186 NAVAL RESEARCH LAB WASHINGTON DC F/G 14/2
STRESS ANALYSIS OF TWO MINI-HAT PRESSURE GAGE DESIGNS.(U)
FEB 82 V J PARKS, R J SANFORD, L A BEAUBIEN
UNCLASSIFIED NRL-MR-4780 NL

END
DATE FILMED
04-82
DTIC

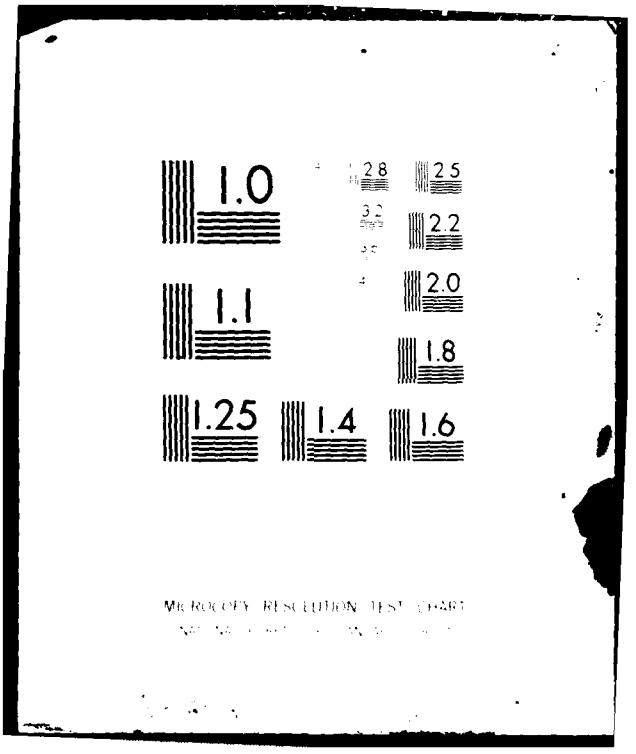
1.0
1.1
1.25
1.4
1.6
2.0
2.2
2.5

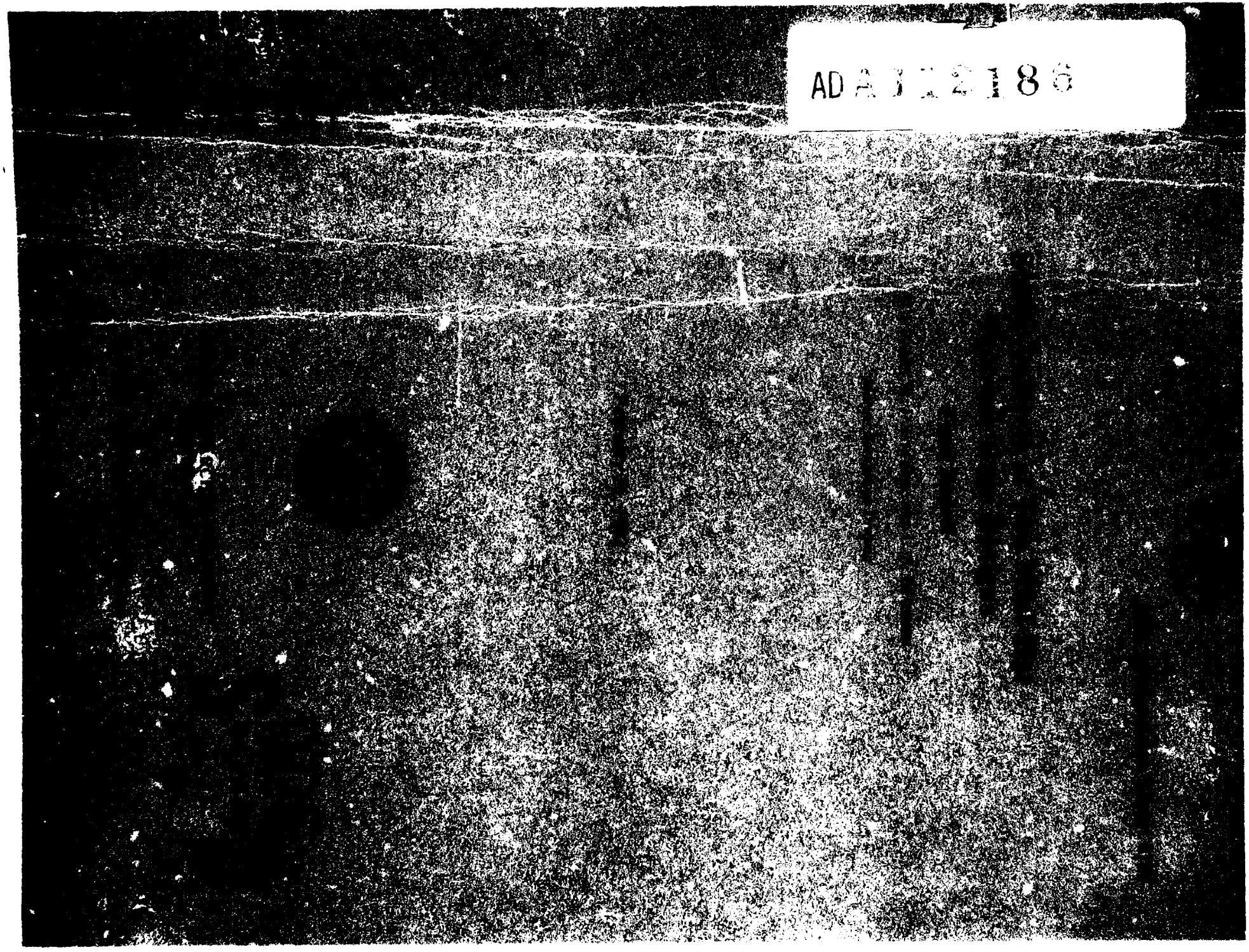

SECURITY CLASSIFICATION OF THIS PAGE (When Data Entered)

REPORT DOCUMENTATION PAGE	READ INSTRUCTIONS BEFORE COMPLETING FORM
1. REPORT NUMBER: NRL Memorandum Report 4780 — 2. GOVT ACCESSION NO.: AD-A112186	3. RECIPIENT'S CATALOG NUMBER:
4. TITLE (and Subtitle): STRESS ANALYSIS OF TWO MINI-HAT PRESSURE GAGE DESIGNS	5. TYPE OF REPORT & PERIOD COVERED: Final Report — August 1979 to March 1980
	6. PERFORMING ORG. REPORT NUMBER:
7. AUTHOR(s): V.J. Parks, R.J. Sanford, and L.A. Beaubien	8. CONTRACT OR GRANT NUMBER(s):
9. PERFORMING ORGANIZATION NAME AND ADDRESS: Naval Research Laboratory, Washington, DC 20375	10. PROGRAM ELEMENT, PROJECT, TASK AREA & WORK UNIT NUMBERS: 1L162618AH80, 58-0286-00
11. CONTROLLING OFFICE NAME AND ADDRESS: Department of the Army, Ballistic Research Laboratory, Aberdeen Proving Ground, MD 21005	12. REPORT DATE: February 26, 1982
	13. NUMBER OF PAGES: 19
14. MONITORING AGENCY NAME & ADDRESS(if different from Controlling Office)	15. SECURITY CLASS. (of this report): UNCLASSIFIED
	15a. DECLASSIFICATION/DOWNGRADING SCHEDULE:

16. DISTRIBUTION STATEMENT (of this Report)

Approved for public release, distribution unlimited.

17. DISTRIBUTION STATEMENT (of the abstract entered in Block 20, if different from Report)

18. SUPPLEMENTARY NOTES

19. KEY WORDS (Continue on reverse side if necessary and identify by block number)

Pressure gage
Photoelasticity
Finite Element

20. ABSTRACT (Continue on reverse side if necessary and identify by block number)

Two designs of mini-hat pressure gages (G-X and J-1) were stress analyzed with three dimensional photoelasticity and a graphics-oriented, axisymetric finite element method. The results were compared with the exact theoretical solution of a pressurized cone. Both methods showed stresses higher than the theoretical solution in the central portion of the cone, and lower than the theoretical solution at the ends of the conical section. The J-1 gage showed a more linear distribution of the stress, in the conical section, than did the G-X gage.

DD FORM 1 JAN 73 1473 EDITION OF 1 NOV 65 IS OBSOLETE
S/N 0102-014-6601

SECURITY CLASSIFICATION OF THIS PAGE (When Data Entered)

STRESS ANALYSIS OF TWO MINI-HAT PRESSURE GAGE DESIGNS

BY
V.J. PARKS
R.J. SANFORD
L.A. BEAUBIEN

ABSTRACT

Two designs of mini-hat pressure gages (G-X and J-1) were stress analyzed with three dimensional photoelasticity and a graphics-oriented, axisymetric finite element method. The results were compared with the exact theoretical solution of a pressurized cone. Both methods showed stresses higher than the theoretical solution in the central portion of the cone, and lower than the theoretical solution at the ends of the conical section. The J-1 gage showed a more linear distribution of stress, in the conical section, than did the G-X gage.

INTRODUCTION

The Ballistic Research Laboratory (BRL) at the Aberdeen Proving Ground, Maryland, has developed and is now using, a conical shaped pressure gage for measuring the gas pressure in large caliber gun barrels. Because of its small size and conical cross section the gage is referred to as a mini-hat gage. Two gage designs, designated G-X and J-1, are shown in Fig. 1. The design of the conical cross section is based on the BRL theoretical solution for the elastic stresses in a hollow cone under external pressure. The gage exhibits a linear response up to 150,000 psi. As a design goal BRL would like to increase this range to 200,000 psi. In support of this effort, the Naval Research Laboratory (NRL) conducted an integrated experimental/numerical stress analysis of the two mini-hat gage designs.

Manuscript submitted January 11, 1982.

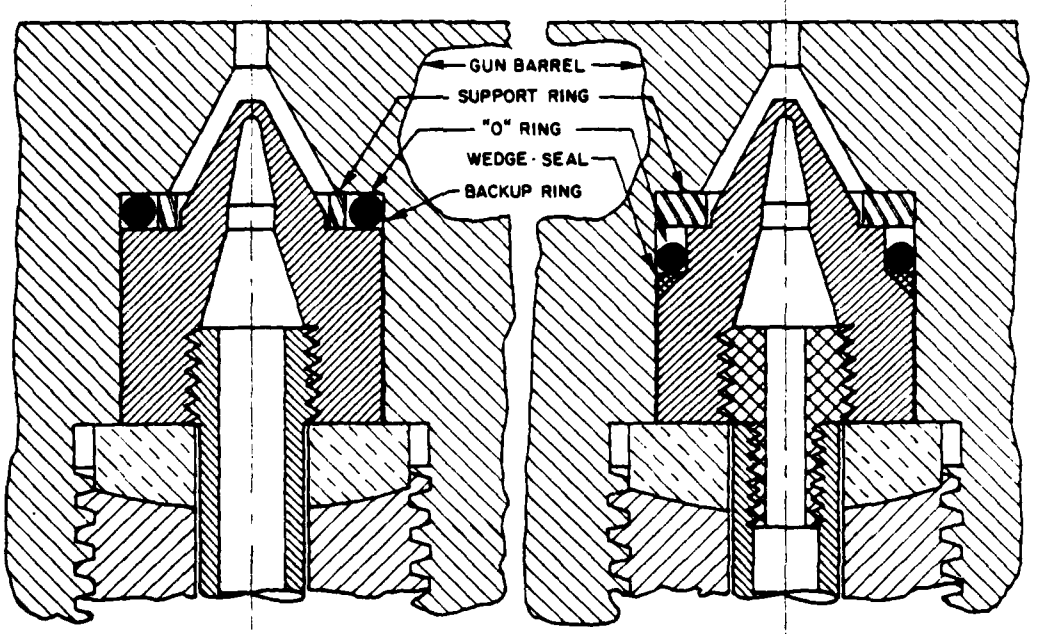

Figure 1 - Assembled G-X (left) and J-1 (right) mini-hat gages.

The G-X and J-1 configurations were studied using three-dimensional photoelasticity and finite-element numerical analysis. Past experience indicates that this integrated approach provides a higher degree of confidence in the results than does either procedure used independently [1]. This is a final report of the NRL studies.

EXPERIMENTAL ANALYSIS

Over-sized models of both gage designs (6.25 times actual size), and the support rings and seals were cast and machined from an epoxy photoelastic material. A cylindrical housing and two plug designs were also cast from the epoxy. The housing and plugs represent the parts surrounding the mini-hat gage. Scaled up O-rings were made from rubber stock. The G-X and J-1 models assembled for loading are shown in Fig. 2.

The epoxy used is a new formulation developed jointly by a stress analyst in industry and NRL [2]. It has machinability characteristics superior to, and can be cast in a much shorter time than, previously used materials. It has a cast surface that when necessary can be used for analysis without machining, in contrast to most previous photoelastic materials [3].

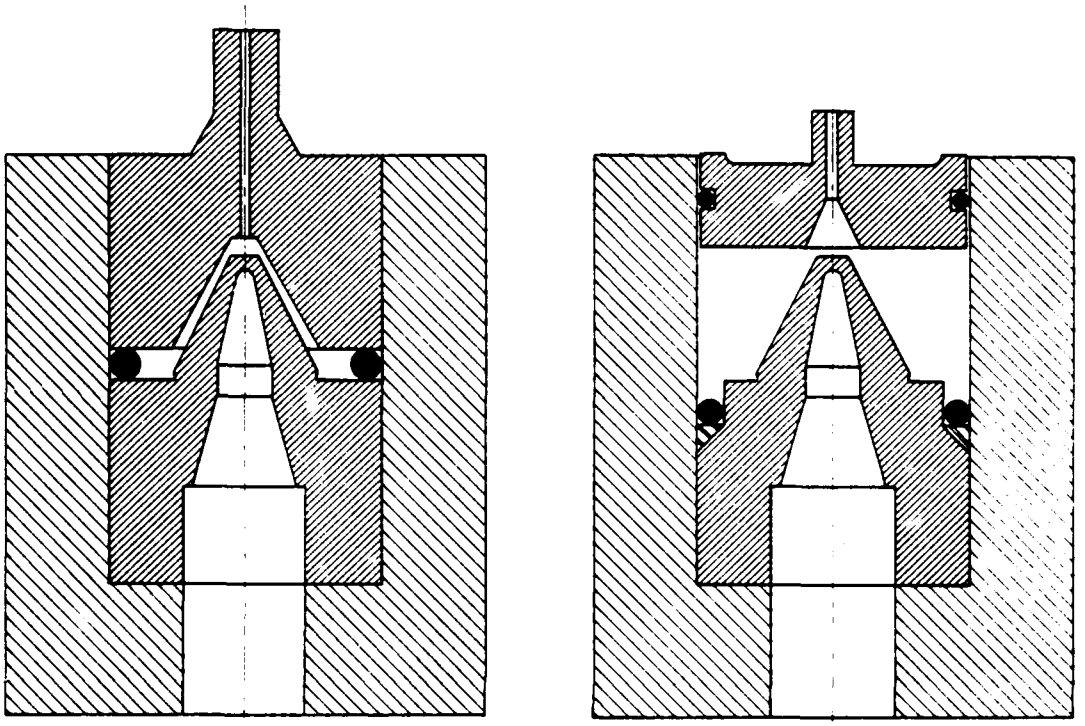

Figure 2 - G-X and J-1 models as assembled for pressure loading.

Prior to actually casting the models an aluminum master of the models, with approximately one millimeter added to all the surfaces, was machined. The master was used as a core to cast a silicone rubber mold. The aluminum master, silicone mold and a finished J-1 model are shown in Fig. 3. The epoxy formulation was mixed, poured in the mold and given a preliminary cure, all following a carefully controlled procedure (full details are available in reference 2).

Following the preliminary curing, both the G-X and J-1 models were machined to final shape from the rough castings. A special form tool was used to machine the inner surfaces of the conical section. The cylinder support rings and plugs were also machined to final dimensions at this stage.

The two machined models were tested separately. Each was placed, in turn, in the cylinder, the O-ring added and the plug with its O-ring added to complete the pressure seal. Each plug contained a small hole and a surrounding stem to inlet the pressure. Each plug was contained in the cylinder, and against the model, with a simple external frame composed of end plates and threaded rods.

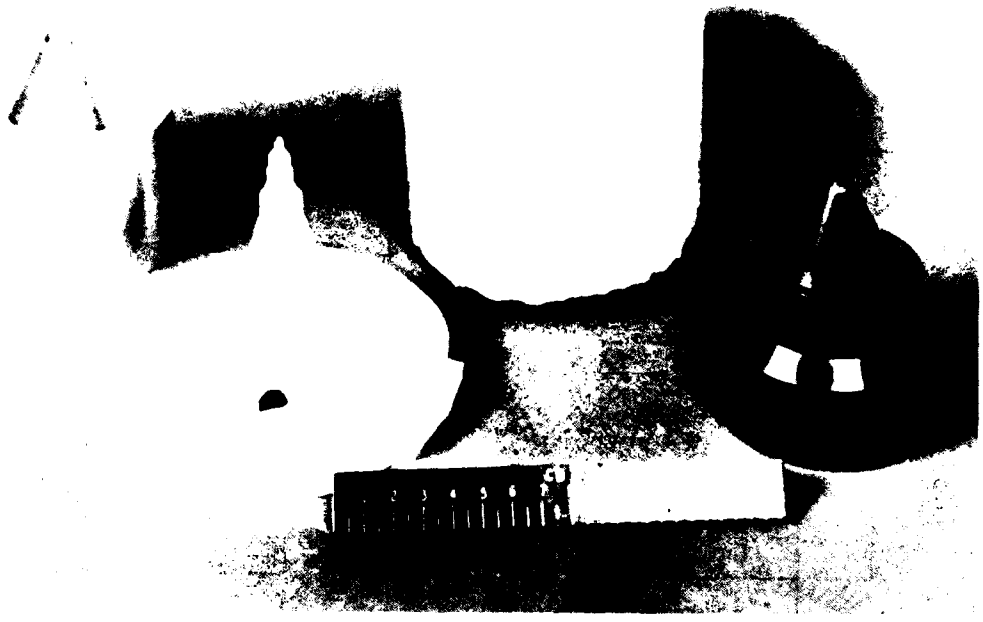

Figure 3 - Aluminum master of G-X (left), inner and outer parts of silicone mold (center) and J-1 model after machining.

The whole assembly (model, O-ring, plug, cylinder and frame), most of which is shown in Fig. 4, was placed in a temperature controlled oven. A hose led from the plug stem to pressurizing equipment outside the oven. Also in the oven was a disk of the same epoxy loaded on its edge with a concentrated force of diametral compression. The stress field of the diametrically loaded disk is known from theory and serves to calibrate the photoelastic response of the material.

The oven temperature was controlled by a cam type programmer. The assembly was heated to the critical temperature of the epoxy (285° F) overnight and remained at that temperature for several hours. This heating cycle completed the curing of the photoelastic material, and simultaneously brought it to the next step in the process; the loading. At the critical temperature the epoxy becomes rubbery (elastic modulus approximately 2200 psi). Low to moderate loads can be used to apply deformation to the epoxy which then can be cooled slowly to freeze-in, or lock-in, the deformation and the corresponding photoelastic response. Slow cooling is essential to avoid thermal deformations which would alter those desired deformations due to the pressure

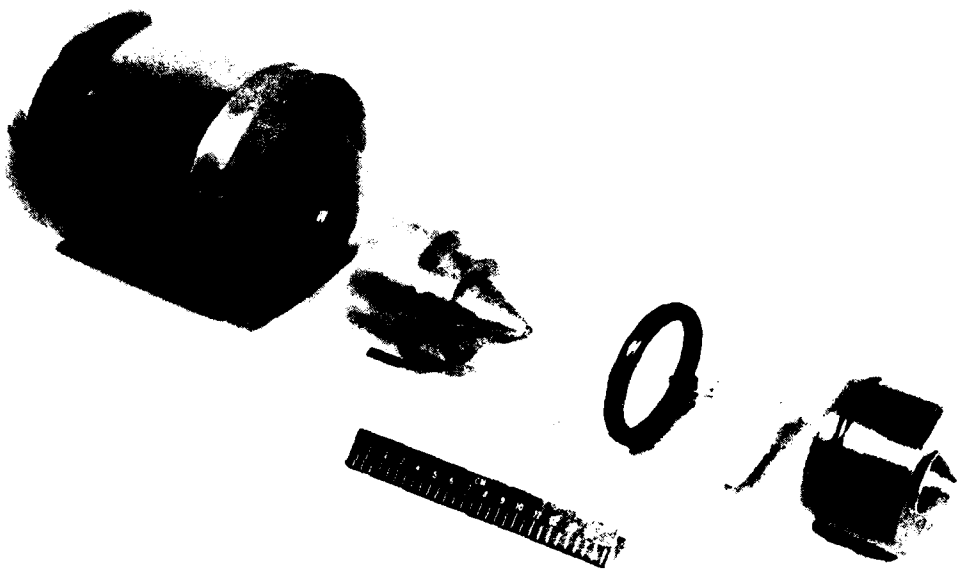

Figure 4 - *Outer cylinder, J-1 model, backup rings, O-ring, support ring and plug (this plug was used in G-X model test).*

load. A regulated pressure load of 25 psi was applied to the system at the critical temperature. The temperature was uniformly reduced to 200°F overnight, at which point the epoxy was again hard, and the deformation locked-in. The assembly was cooled to ambient temperature, the pressure vented and the model removed from the assembly. A meridian slice was cut from each model. Fifteen hoop slices were taken from the G-X model, and sixteen from the J-1 model. The slices were cut, for the most part, with a 0.050" thick circular milling cutter. Most of the slices were between 0.100" and 0.120" thick. The slices and the remaining parts of the G-X model as well as a calibration disk are shown in Fig. 5.

All slices and calibration disks were photographed in both dark-field and light-field arrangements of a diffused, sodium-light, 12" diameter, polariscope.

Fig. 6 are dark- and light-field isochromatic patterns of the meridian slices from the two models. Fig. 7 are dark- and light-field isochromatics of the hoop slices in the upper conical section from both models.

Figure 5 - Photoelastic model of the G-X mini-hat gage after being sliced for analysis. The photoelastic calibration disk is shown in the upper left.

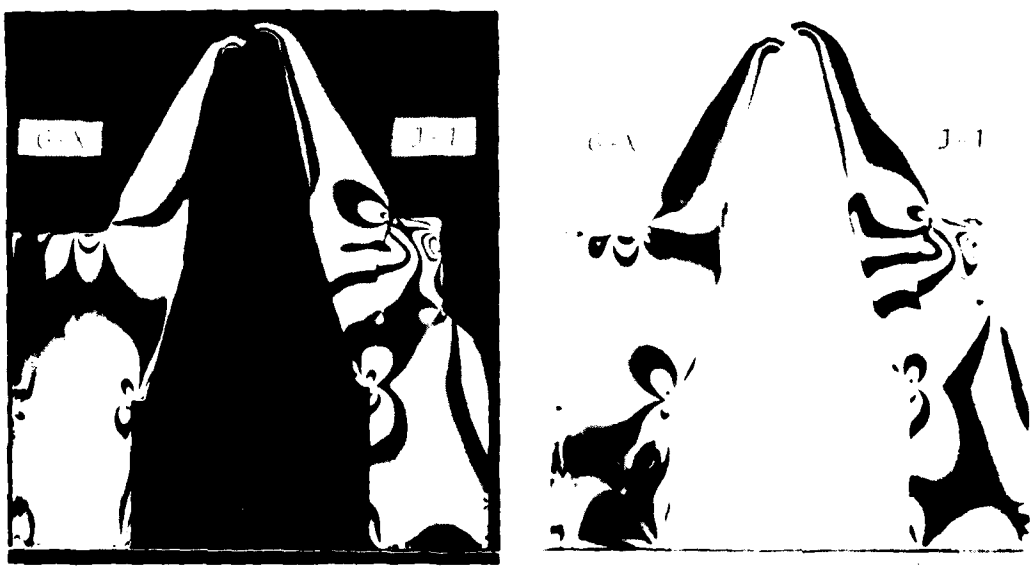

Figure 6 - Dark and light field isochromatic patterns of the meridian slices cut from the G-X and J-1 models.

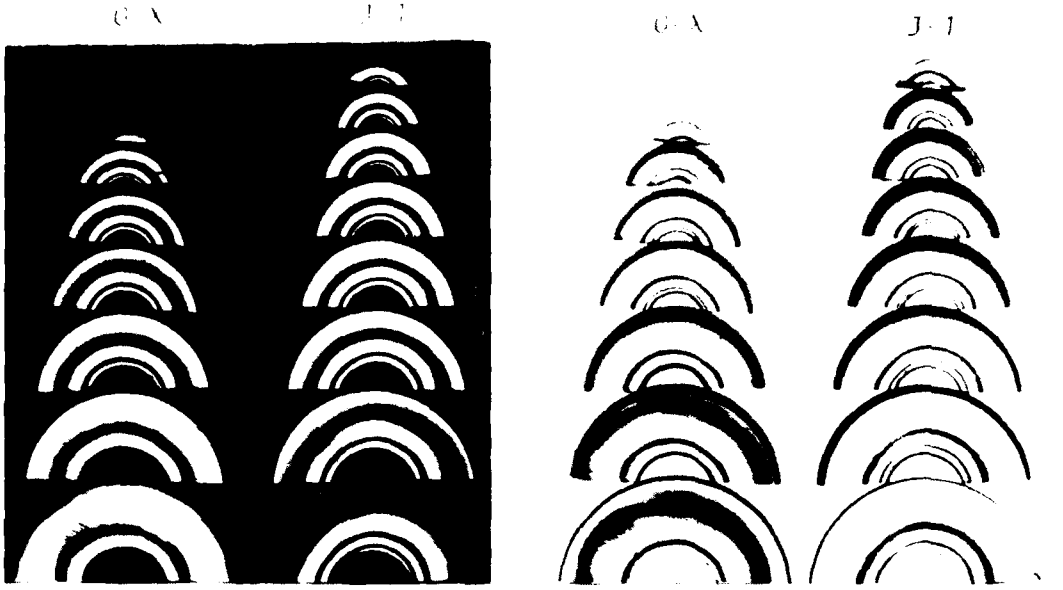

Figure 7 - Dark and light field isochromatic patterns of the hoop slices cut from the upper conical sections of the G-X and J-1 models.

The relation of isochromatic fringes to stresses in the model is defined by the stress-optic equation as

$$\sigma_1 - \sigma_2 = \frac{nf}{t} \qquad (1)$$

where

σ_1 and σ_2 are the principal stresses in the plane in which the fringe is being viewed

n is the fringe order at the point on which σ_1 and σ_2 act

t is the optical thickness of the slice, at the same point, in the viewing direction

f is the material fringe value (the photoelastic constant).

On free boundaries (boundaries with no applied force or pressure) the relation reduces to

$$\sigma_t = \frac{nf}{t} \qquad (2)$$

where

σ_t is the tangential stress on the boundary in the plane in which the fringe is viewed.

Material fringe values were obtained for each test, using the known theoretical solution for the stresses at the center of the calbriation specimen in diametral compression. The f-values were 2.15 psi-in/fringe for the G-X model material and 2.12 psi-in/fringe for the J-1 model material.

In most analyses, including this one, the integral fringe orders in the dark field photographs and the half-order fringes in the light field photographs are easily established in a number of ways. Fractional fringe values down to about one-hundredth of a fringe order can then be determined at given points.

Fringe orders along the inner 12.3° conical surface on both the meridian slice and the hoop slices were estimated to 0.01 fringe. The hoop and radial stresses were thus determined using Eqs. (1) and (2), and normalized in terms of the applied 25 psi pressure. The normalized radial and hoop stresses for the G-X and J-1 models are reported in Figs. 8 and 9, respectively. The exact theoretical solution for the stresses in a pressured cone is shown for comparison.

The radial stresses were obtained directly from Eq. (2). The hoop stresses required a somewhat more involved analysis, and some comments may be in order. The hoop slices were cut perpendicular to the axis of the gage, first to simplify cutting and also to maintain the radial symmetry of the fringe patterns. Those slices with tapers on the edge, when viewed normal to their surface, had two difficulties: first they produced a shadow at the edge, and second, they introduced a non-zero stress normal to the edge, thus reverting from Eq. (2) back to Eq. (1). Most of these slices were photographed two ways; normal to their surface (as shown in Fig. 7) and with the viewing direction tangential to the tapered edge. Because the second type of photograph gave elliptical fringes, it was decided to analyze the first type (with circular fringe shapes) using Eq. (1). This required that the two difficulties mentioned above be taken care of. To circumvent the edge shadow, the radial position of integral and half order fringes was estimated and these values plotted and the curve extrapolated to the center of the shadow to estimate the fringe order at the boundary. Because the fringes were of circular shape this could be done over a wide arc up to an angle of almost 180° as seen in Fig. 7. In practice the centerline of each photoelastic fringe was matched to a circle and the radius taken.

Because the angles were 12.3° and 15.7° the second difficulty introduced only a small variation. Consider σ_A and σ_B in Fig. 10. The stress on the inner boundary in the meridian plane varies between zero and the radial stress value. At 12.3° σ_A theoretically on the inner bending is about 2.5% of the hoop stress σ_B. At 15.7° it is about 3.5% of the hoop stress. The stress difference determined from the hoop slices and Eq. (1) was adjusted by these percentages to obtain a best estimate of the hoop stresses.

Fig. 10 shows the distribution of the stress difference in the G-X model along lines perpendicular to the model axis at various heights, in the conical section. This result was taken from the same curves mentioned above, that were used to extrapolate to the boundaries. Eq. (1) was used to obtain the stress difference. The comparable theoretical stress difference was taken fro the exa t solution for stresses in a pressurized cone.

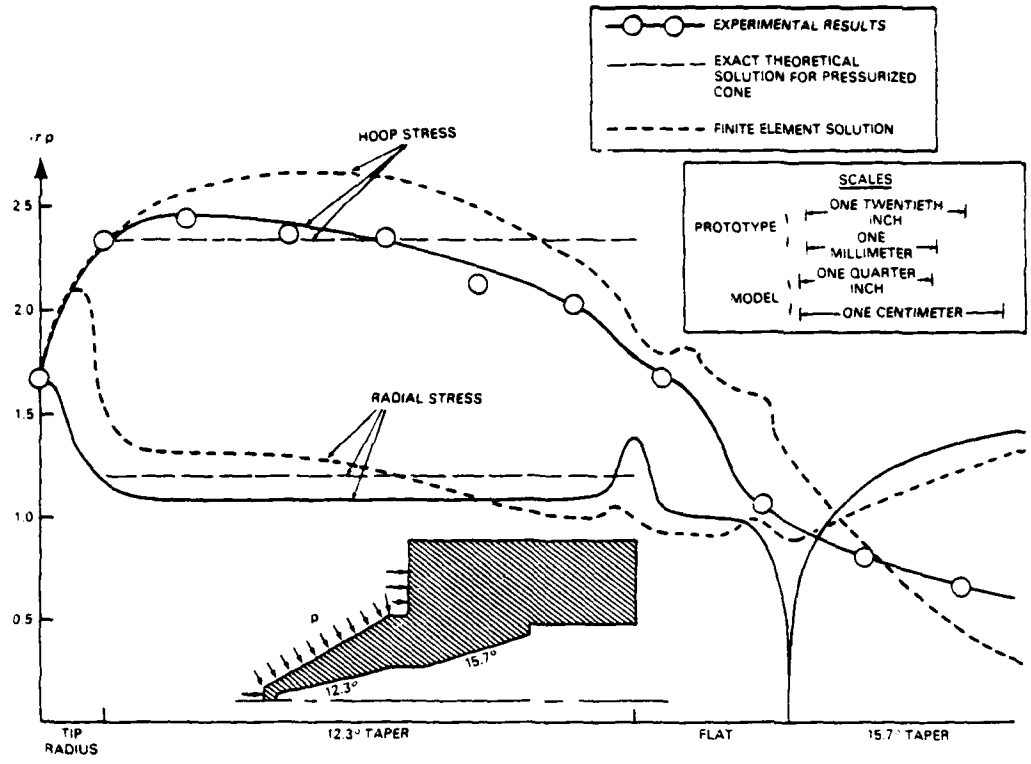

Figure 8 - Normalized radial and hoop stresses along inner boundary at the upper section of the G-X mini-hat gage. Exact theoretical solution for pressurized cone and finite element solution are added for comparison.

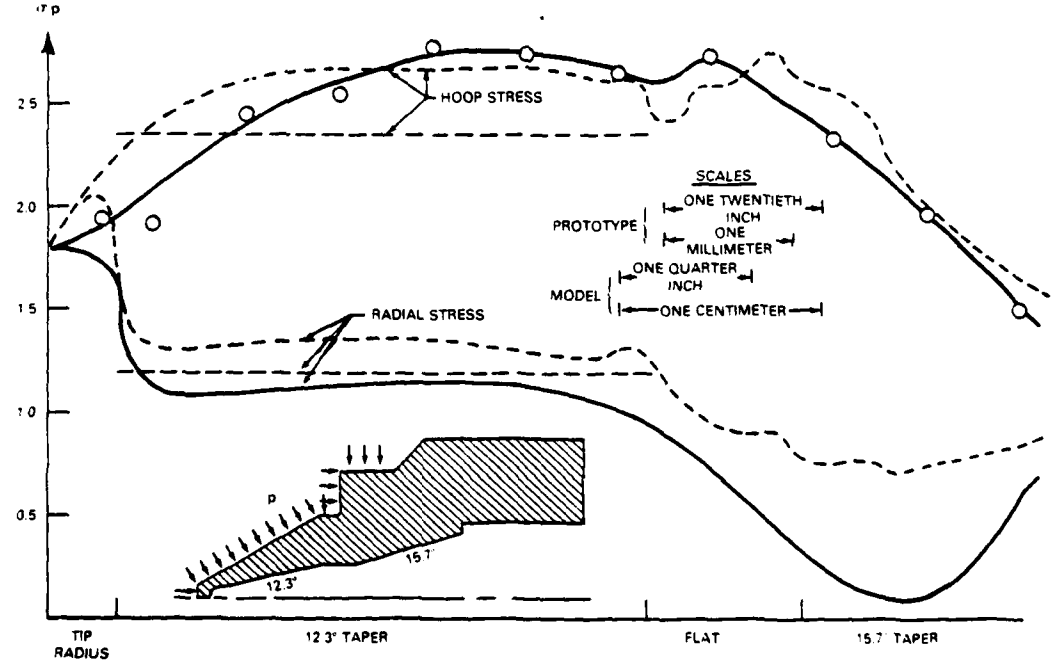

Figure 9 - Normalized radial and hoop stresses along the inner boundary of the upper section of the J-1 mini-hat gage. Exact theortical solution for pressurized cone and finite element solution are added for comparison.

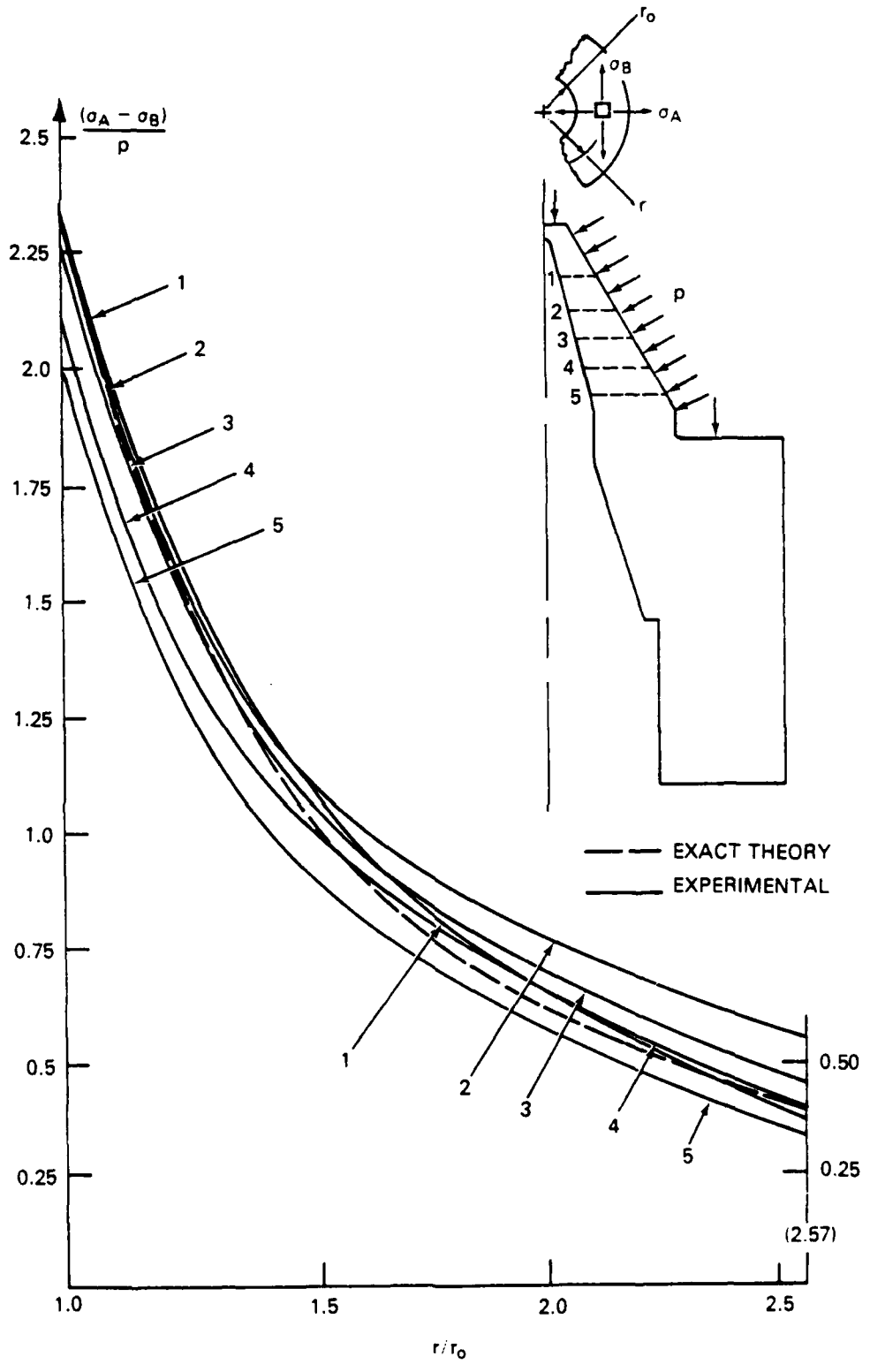

Figure 10 - Normalized stress differences in the conical region in the plane perpendicular to the axis of the G-X mini-hat gage. Exact theoretical solution for pressurized cone is added for comparison.

NUMERICAL ANALYSIS

The primary objective of the numerical analysis was to determine and graphically display the principal stress distributions in the conical sections of the G-X and J-1 gage configurations. Secondary objectives were correlation of numerical and experimental results and verification of experimental boundary conditions as a representation of prototype loading. The integrated nature of the combined experimental/numerical approach allowed optimal use of both methods. An initial numerical solution was used in determining the intensity of loading for the experimental model. Subsequently, experimental stress patterns were used to refine the local distribution of loads for the numerical model.

SIMULATION SYSTEM

The parametric finite element analysis was performed using an NRL developed interactive, graphics-oriented package called TOTAL (Two-dimensional Orthotropic Timesharing Analysis Library) [4]. This library consists of a set of modular programs linked by a broadly structured disk-file data base. Each of the thirty-plus programs implements a specific task in the modeling/solution/interpretation procedure, and creates data files to be used as needed by other programs further along the simulation path. All of the programs are auto-prompting and to a considerble extent auto-instructional, with all the intricacies of data file manipulation hidden from the user. Many of the programs embody extensive interactive graphics capabilities, some of which are unique to the TOTAL system.

The use of modular programs is intended to encourage numerical experimentation (or parametric analysis). For example, complete or partial changes in files containing boundary conditions, material properties or geometric information can be quickly made by programs made to perform specific modification tasks. The problem can then be resolved without reentering those quantities which did not change. Similarly, compatible result files can be linearly combined to study the effect of superposed solutions. These features were utilized extensively in this study.

MODELING AND SOLUTIONS

Since the two configurations were identical except for the removal of some material in the J-1 case, it was possible to base both geometry models on a basic J-1 mesh (Fig. 11a) with 457 nodes and 796 elements. The G-X configuration (Fig. 11c) was then modeled by linking on a small region (Fig. 11b) to form a mesh with 499 nodes and 876 elements. These geometries were used for all studies, both axisymmetric and two dimensional (plane stress/strain).

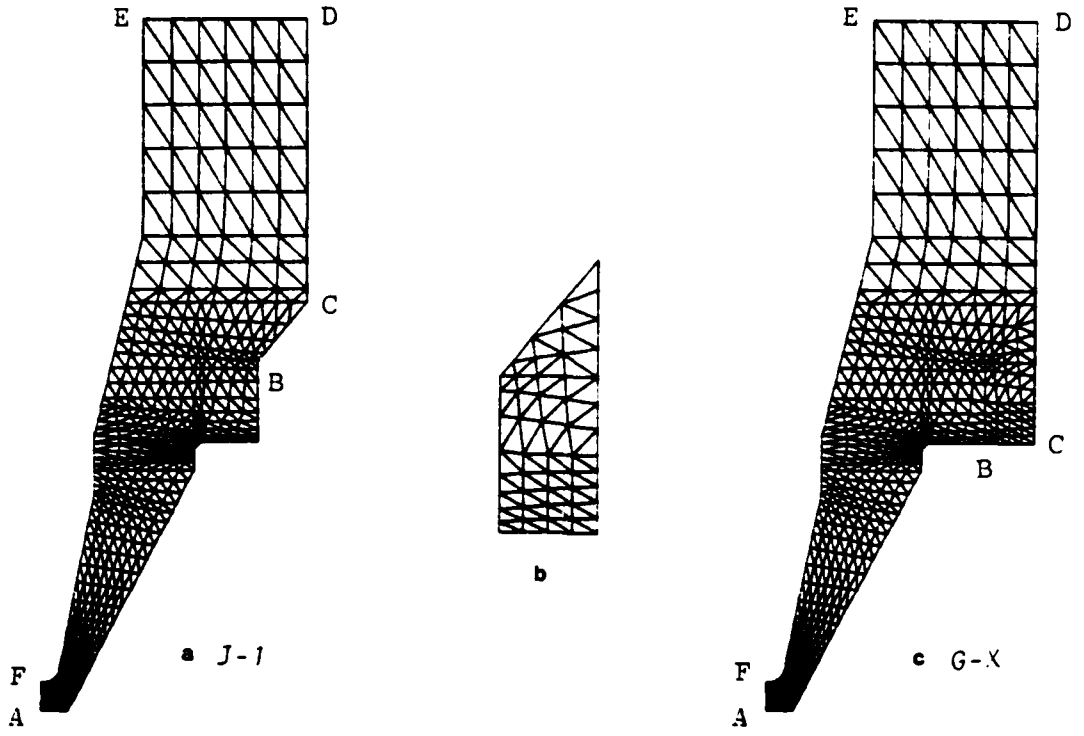

Figure 11 - Numerical model meshes.

For both configurations the primary loading consisted of a uniform hydrostatic pressure applied to the outer surface of the gage up to the point of O-ring seal B. (This loading is equivalent to that used in the experimenal study). In addition, various loads in the vicinity of and caused by the O-ring itself were also applied. Choice of the intensity and distribution of these local loads varied with different solution objectives (e.g., prototype or photoelastic model simulation), and is described in greater detail in Appendix A. However, a reference prototype loading was chosen consisting of an extension of the hydrostatic pressure from the sealing point B to the maximum outer radial point C in both configurations, and all results described below use this reference loading. For all solutions, points along edge DE were constrained in the axial direction but free in the radial direction, and points along the axis edge FA were free in the axial direction.

Two basic material property cases were used, a prototype condition (E=30000000 psi, Poisson's ratio=.3) and a photoelastic model condition (E=2200 psi, Poisson's ratio=.35-.495).

The results summarized below are based on one axisymmetric solution for each configuration using prototype material and loading conditions. However, the full study consisted of dozens of solutions, both axisymmetric and two dimensional. From these solutions over a hundred graphical displays were generated and evaluated to study such variables as the sensitivity of the numerical model to various parameters and the correlation of numerical and photoelastic results. Various combinations of the basic loading with local loads near the O-ring were tried to improve correlation with experimenal results, and to determine whether differences in stress distribution in the two configurations were due to geometry or seal-related loading changes. Sensitivity of the numerical modeling of the photoelastic experiment to values of Poisson's ratio approaching 0.5 (the value of the photoelastic material) were studied. Also, the validity of two dimensional (plane stress/strain) analysis of the problem was investigated.

GRAPHICAL NUMERICAL RESULTS

The primary results of the numerical analysis are presented in graphical form in Figs. 12 through 16 for both the G-X and J-1 configurations due to the reference prototype loading. In Figs. 12 and 13, plots are given of non-zero (hoop and radial) principal stress distributions on the inner surface of the two gage geometries. It is evident that there is a more uniform distribution of boundary stresses (and strains) over a longer segment of the interior conical surface in the J-1 configuration.

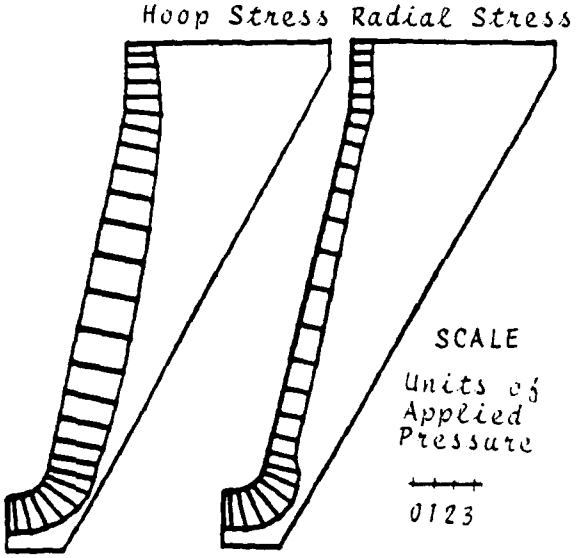

Figure 12 - Interior surface stresses for conical region of G-X.

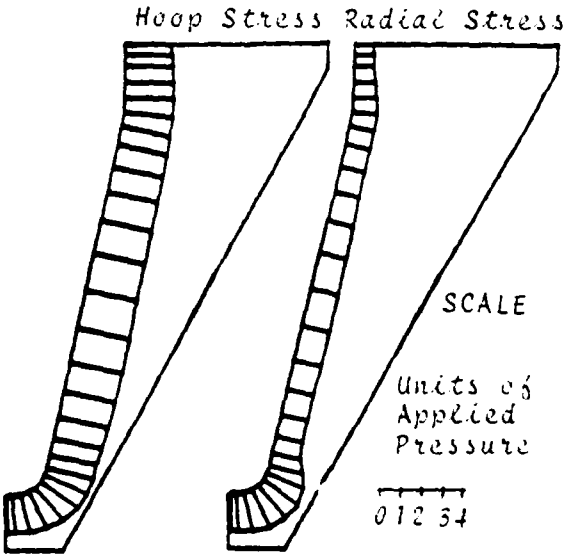

Figure 13 - Interior surface stresses for conical region of J-1.

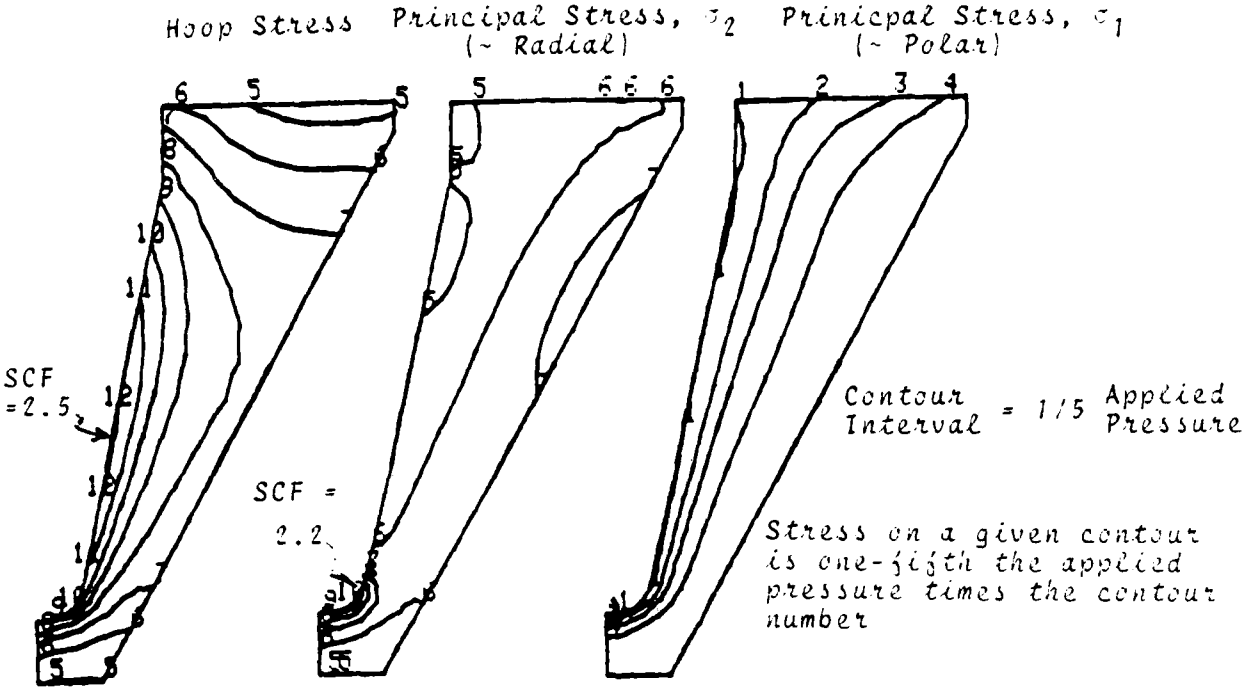

Figure 14 - Principal stress contours for conical region of G-X.

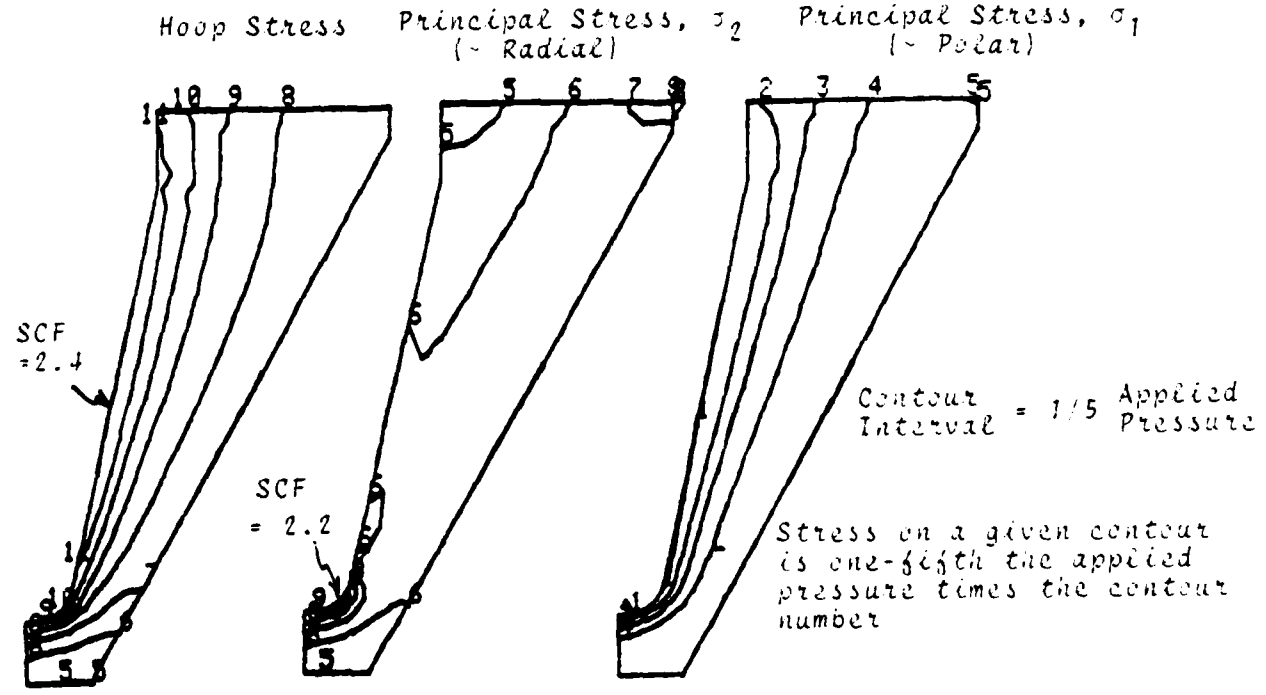

Figure 15 - Principal stress contours for conical region of J-1.

The next two Figs. (14 and 15) show contour plots of principal stresses in the two configurations, with indication of values and locations of maximum stress concentration factors relative to the applied pressure. The essentially parallel nature of the stress contours in the conical region agrees generally with the theoretical solution, with the J-1 configuration exhibiting a more extended region of such behavior. However, relative stress concentrations in the two geometries do not appear to predict any superiority of the J-1 over the G-X with respect to linear behavior as a gage.

Finally, exaggerated overlayed displacement plots for the two geometries are given in Fig. 16. It is seen that in the conical region the inner surface of the J-1 configuration shows less curvature under load that the G-X, probably due to the removal of some rotation-restraining material from the base.

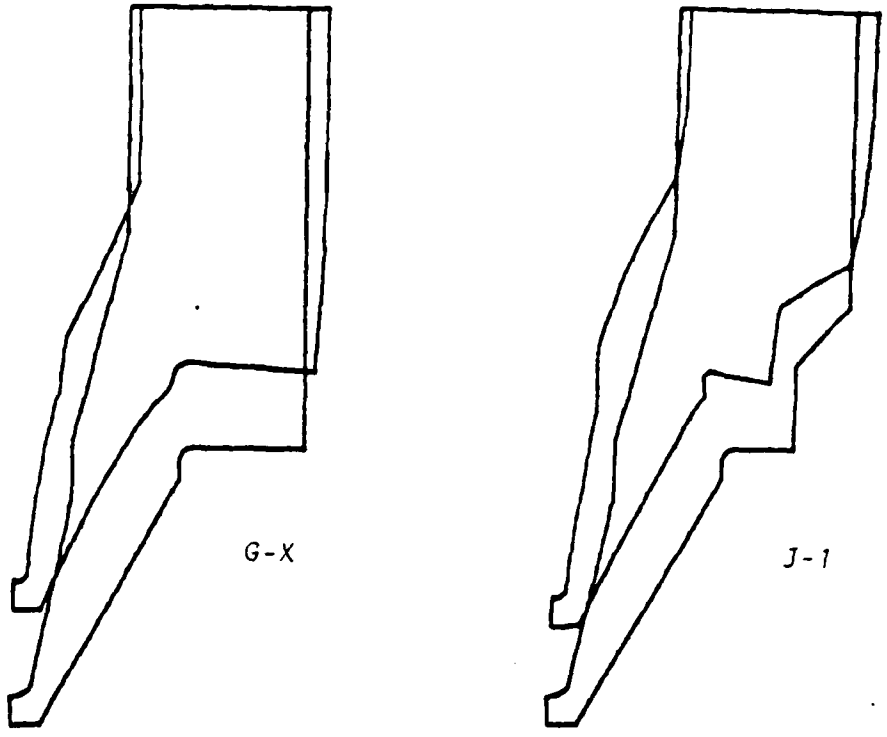

Figure 16 - The deformed cross sections, magnified 500 times, overlayed on the undeformed cross sections.

DISCUSSION

The experimental and numerical results are in reasonable agreement with the theoretical solution of the stresses in a pressurized cone. The primary variations occur at the ends of the cone. At the small end, the cone is truncated with an approximately spherical cap, and the hoop and radial stresses, perforce merge. At the large end, the cone is truncated by a cylinder. The changes on the outer surface are more pronounced than the on the inner surface and tend to reduce the compressive hoop stresses in the G-X design, while the compressive hoop stresses in the J-1 design remain more uniform. This difference in the hoop stress between the two models is apparently due to the reduced stiffness of the J-1 meridian cross section compared to the G-X cross section, and the extended region of pressurization in the J-1 design. From the criterion of uniform stress, in the conial section, it would appear that the J-1 is superior to the G-X.

APPENDIX A

EFFECT OF THE O-RING SEAL LOADING. The high pressures seen by the prototype geometries, combined with the differences in stiffness of the steel and rubber, result in a nonlinear deformation of the circular cross-section of the O-ring into an approximately rectagular shape, with resulting uniform (hydrostatic) pressure along all bounding faces. This effectively extends the uniform pressure loading from the initial sealing point B to the outer radial point C (Fig. 11), thereby producing the loading chosen as the reference prototype loading.

In the photoelastic model of the J-1 gage, the approximately equal stiffness and nonlinear behavior of the O-ring and the adjoining material are such that the small pressure required to generate a reasonable number of photoelastic fringes results in a contact loading that differs from the prototype. Highly localized radial side thrusts can develop in the sealing region due to two mechanisms. The first is a radial squeezing action caused by insertion of a slightly oversized ring, independent of the applied pressure. The second mechanism, constraint of the lateral expansion of the O-ring cross-section as pressure is applied, can produce a side thrust whose value and distribution vary with increasing applied pressure. The existence and location of photoelastically generated fringes in the region of O-ring contact appeared consistent with the presence in the experiment of local radial loads due to the insertion mechanism only.

The added effect of an extra, experimentally-generated radial load was modeled numerically . Increasing increments of local radial forces, applied at a point indicated by the experimental results, were added to the basic uniform pressure. For each increment, plots of the resulting principal stresses on the interior surface were visually compared with equivalent experimental curves. This procedure resulted in improved numerical/experimental correlation of the overall stress distrbution, but there was very little change in the primary-interest conical region.

It was concluded that some local discrepancies between the numerical and experimental results were attributable to the presence in the experiment of an extra O-ring loading which would not be present under in-service conditions, but that this extra load would have little effect on the distribution of experimental stresses in the concial region of the J-1 gage configuration.

REFERENCES

1. Sanford, R.J. and Beaubien, L.A., "Stress Analysis of a Complex Part: Photoelasticity vs. Finite Elements," Experimental Mechanics, Vol. 17, No. 12, December 1977, pp. 441-448.

2. Parks, V.J., Sanford, R.J. and Cernosek, J., "Analysis of Turbine Blades Using a Rapid 3-D Photoelastic Method," Journal of Aircraft (AIAA), Vol. 18, NO. 3, March 1981, pp. 213-219.

3. Parks, V.J. and Sanford, R.J., "Three-Dimensional Photoelastic Stress Analysis of the Dovetail Region of the TF-30 Turbine Engine Third-Stage Fan," NRL Report 8276, December 1978.

4. Beaubien, L.A., "TOTAL: Interactive Graphics System for the Two-Dimensional Analysis of Linear Elastic Systems," Structural Mechanics Software Series, Vol. 1, N. Perrone and W. Pilkey, University of Virginia Press, Charlottesville (1977).

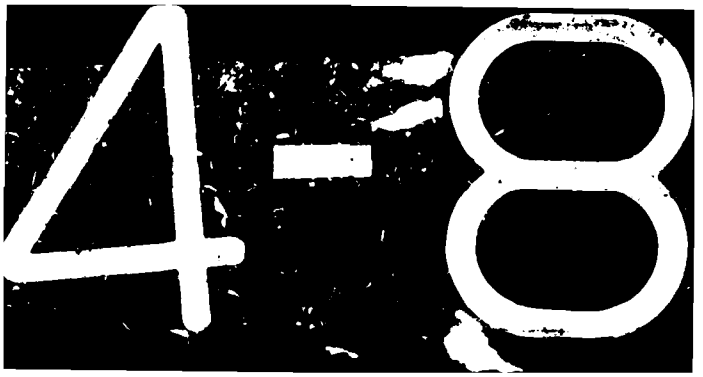
4-8